Research Article

Xingjun Wang, Quanmin Xie, and Ying Huang*

Study on the frequency of acoustic emission signal during crystal growth of salicylic acid

https://doi.org/10.1515/ntrev-2021-0042
received March 28, 2021; accepted June 7, 2021

Abstract: Based on the results of the previous experiment, this article studied the acoustic emission (AE) signals released during the crystallization of salicylic acid to establish the relationship between the AE signal and the particle size. A tremendous amount of acoustic data was analyzed using time–frequency domain analysis methods in order to extract the valuable contents. Based on the diffusion theory, the vibratory model between the AE signal and the crystal particle size was established. This article mainly studies the process of small particles diffusing to the growth point by impact, adding to the lattice, and the crystal releases energy. The impact of the growth unit on particle aggregate is equivalent to a linear elastic vibration system with one end fixed and the other end free. The vibration frequency is 200–355 kHz when the particle size is between 600 and 1,100 μm. The calculated vibration frequency is in good agreement with the measured frequency.

Keywords: salicylic acid, acoustic emission, particle size, crystal growth

1 Introduction

Crystallization is an important step significantly affecting the final product characteristics, such as particle size and its distributions [1], shape, and purity [2,3]. Crystalline particle size is usually the key requirement of the drug crystallization process, which not only affects the performance of the final product but also affects the operation and product characteristics of downstream products [4]. Some factors (temperature, stirring, impurities, and external field) affect the size of nucleation by affecting the metastable state of the solution. On the one hand, with the increase of temperature, the interaction process between particles is accelerated; on the other hand, the process slows down with the decrease of saturation. Therefore, it is a complex process. Vibration and stirring increase all kinds of collisions and impact a supersaturated solution resulting in a high supersaturated area, which accelerates the fine crystal nucleus in the solution. In addition, magnetic field, radioactive ray, and roentgen ray have influences on the nucleation rate of the solution. The anisotropic growth was studied [5]. The effect of ultrasound on supersaturated solutions mainly depends on the power and intensity of radiation. X-ray, infrared spectroscopy, and electron diffraction methods were used to analyze the crystal structures [6]. The microstructure and the thermal behavior of the deformed disks have been studied by differential scanning calorimetry [7,8]. Different particle sizes could change the properties of microstructure [9]. Some traditional methods of measuring particle size, such as focused beam reflectance measurement (FBRM) [10–12], laser diffraction [13,14], mass spectrometry [15], and pressure fluctuations [16], need clean test environment. Subero-Couroyer *et al.* used the reaction crystallization method to generate SA microparticles (5 μm) in the suspension and then controlled agglomeration to increase its size to improve downstream solid processing operations [17]. Hatkar and Gogate studied the effect of additives on the crystallization process at a given supersaturation level. They considered that the change of particle size is due to the change in supersaturation [18]. Seidel and Martins studied the effect of the change of antisolvent crystallization conditions on the size and shape of SA crystal under thermal gradient [19,20]. Caro *et al.* studied the effects of process conditions (*i.e.*, stirring speed, feeding point, reactant concentration, and vessel diameter) on the size of SA crystal after reactive crystallization [21]. However, many chemical production processes are

* **Corresponding author: Ying Huang,** The College of Aviation Engineering, Taizhou University, Taizhou, 318000, China; Sorbonne Universités, Université Pierre et Marie Curie, Paris 6, Institut Jean le Rond d'Alembert, CNRS UMR 7190, Case 162, 4 Place Jussieu, 75252, Paris Cedex 05, France, e-mail: ying.huang2014@qq.com
Xingjun Wang: Key Laboratory of Mechanics on Disaster and Environment in Western China, The College of Civil Engineering and Mechanics, Lanzhou University, Lanzhou, 730000, China
Quanmin Xie: Hubei Key Laboratory of Blasting Engineering, Jianghan University, Wuhan, 430056, China

often carried out under hard process conditions, such as high pressure, high temperature, corrosive medium, dust content, and non-real-time technique.

Wang *et al.* used acoustic emission (AE) monitoring to explain the relationship between AE variables and the development of crystallization mechanism from a new perspective so as to better understand crystallization phenomena (such as nucleation, growth, and agglomeration) [22,23]. In addition, by monitoring the vibration signal released during the crystallization of salicylic acid, the effect of the injection rates on the particle size distribution was studied [24]. AE method has some advantages compared with these methods. One of the main advantages of AE technology is that its sensor does not need to be placed inside the reaction equipment (*e.g.*, reactor, dryer, grinder, grinder, and crystallizer). Because of its nonintrusive and nondestructive features and due to the possibility of real-time information collections, AE might be a very attractive technique for the development of online monitoring and control systems. It has been applied in various areas of research and industrial process monitoring, such as plastic strain mechanisms [25], tablets [26], slurries [27], powder blending [28], heterogeneous reactions [29,30], various fluidized bed processes [31–34], ice-melting [35], fiber fracture [36], endpoint detection in high shear granulation [37–40], and phase transition [41]. However, few studies deal with the AE monitoring of crystallization processes [42–44].

In recent times, the AE technology and its vibration model in the process of crystal nucleation are the research hot spot in related fields, which has significant research value for the development of online monitoring system. The novelty of this study is to use a physical model to set up the corresponding relationship between AE frequency and particle size by analyzing the collected AE signals. Previous studies showed the presence of AE signals during crystallization [22]. As the relation between the AE frequencies and particle sizes has not yet been explicated in the literature for this phenomenon, the vibration behavior of laminated composite plates was studied [45–49]. Thanks to Landau Lifchitz, *Theory of Elasticity: Volume 7* (*Theoretical Physics*) Chapter: 25, this research is to set up the relation between the fundamental (lowest) natural frequency in function of the size of the crystals. The result can use the parameters of AE frequencies to measure the mode of crystallization growth. Generally, the crystal structure grows from nanosize to micrometers. The results of this research give a new method to study nanocrystallization [50–53] molecular dynamics simulation [54].

The rest of this article is organized as follows. Section 2 briefly introduces the main features of hits and defines the AE signal parameters in the specification. Section 3 presents the crystallization device and signal acquisition equipment used in this study, as well as the parameter setting and working principle of the equipment. The mechanical model is used to calculate the frequency of the AE signal released during the growth of the salicylic acid crystal in Section 4. Such calculation is based on the elastic theory of theoretical physics course. To obtain further information and views on the crystallization process, the experimental results are further explained in Section 5. Finally, the article concludes with a discussion of further research direction.

2 Introduction to AE

As shown in Figure 1, the AE parameters can be measured to avoid recording too large number of data. For example, a threshold power ratio value (40 dB) has to be used from "blank" measurements to evaluate the level of insignificant signals emitted by the stirring system, the electromagnetic environment, and the flow of the liquid in the crystallizer. In this study, the counts and the peak frequencies of AE signal were used. The counts are defined as the number of times the emission acoustic signal crosses the detection threshold. There are 18 counts in Figure 1. The peak frequency is defined as the point in the power spectrum at which the peak magnitude occurs. The real-time fast Fourier transform is performed on the waveform. The peak frequency contains the largest magnitude of AE hit.

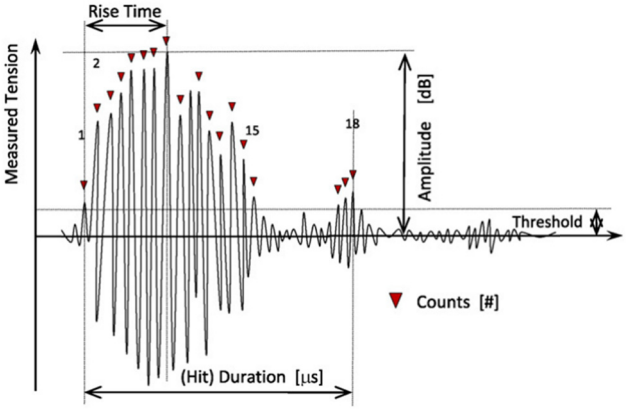

Figure 1: The characteristic parameters of a emission acoustic signal.

3 Experiment

Figure 2 shows the schematic diagram of the crystallization device used in this study. Two flat-bottom jacketed 1 L glass containers are connected by a peristaltic pump (Watson 313S), and sulfuric acid solution (H_2SO_4) in No. 1 glass is added into the reactor (No. 2 glass). A high-efficiency propeller (mix TT TM) is set in the mold, with a rotating speed of 200 rpm. The reactor is a cylindrical vessel with a diameter of 0.11 m and a maximum height of 0.2 m. The gap between the agitator and the bottom of the reactor is 0.03 m. The injection point is located in the liquid midpoint between the agitator position in the center of the reactor and the reactor wall.

The AE signal is detected by the piezoelectric sensor (physical acoustics company, wd-fs62), which is fixed on the outer wall of the reactor. To improve the transmission efficiency of AE signal, coupling grease is used between the glass wall and the sensor. Then, the data acquisition system (DAS of European physical acoustics company) is used to adjust, amplify, filter, and process the signals collected by the detection equipment. To avoid the interference of the background signal, the detection threshold is set higher than 40 dB. Please refer to the author's previous articles [24] for the parameter setting of our experimental AE equipment.

The whole experimental process is continuously monitored by AE equipment, which starts to work before sulfuric acid is introduced. At the end of the intermittent process, SA suspension samples are extracted from two sampling points of the crystallizer for offline size measurement. During the whole experiment, the temperature of the reactor is controlled at 20°C by manipulating the set-point temperature of the heating tank. The sulfuric acid solution is prepared in reactor 1 and added to the sodium salicylate solution at an injection rate of 20 mL/min. The concentration of the latter is 0.2 mol/L, which was initially prepared in No. 2 glass reactor.

4 Experimental results and discussion

The AE signal emitted by developing slurries consists of a mixture of many waves, spread over several orders of magnitude. This is why the recorded AEs frequency spectra are generally complex. The time–domain analysis is used to grasp the macro distribution of the data, but the small changes in the data are not easy to observe. To evaluate these parameters as a function of the basic mechanism of crystallization, the time–frequency analysis method is used. This technique studies a two-dimensional signal in both the time and the frequency domains simultaneously.

The results of the previous experiment are reviewed to reveal the relationship between the AE signal and the corresponding crystallization phenomenon. For example, as shown in Figure 3, the first time period, from 0 to 200 s, the sulfuric acid solution (H_2SO_4) is added into the reactor. No crystallization is observed, and the count of emission acoustic is almost zero. In the second time period, from 200 to 600 s, crystallization is observed and the count increases. In the third time period, from 600 to

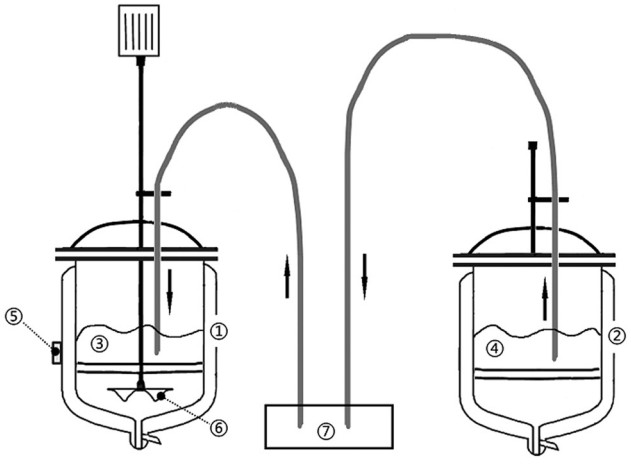

Figure 2: Experimental setup for the semi-continuous precipitation of salicylic acid. (1) 1 L glass 2 reactor, (2) 1 L glass 1, (3) R_Na, (4) H_2SO_4, (5) acoustic emission sensor, (6) stirrer, and (7) pumper.

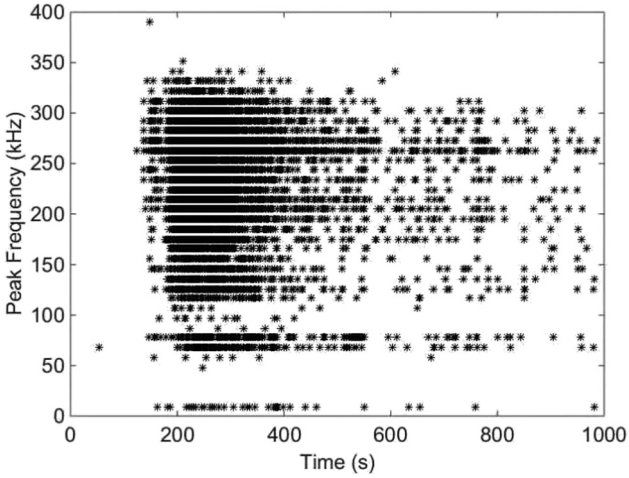

Figure 3: Time variations of the individual peak frequencies during the crystallization of salicylic acid.

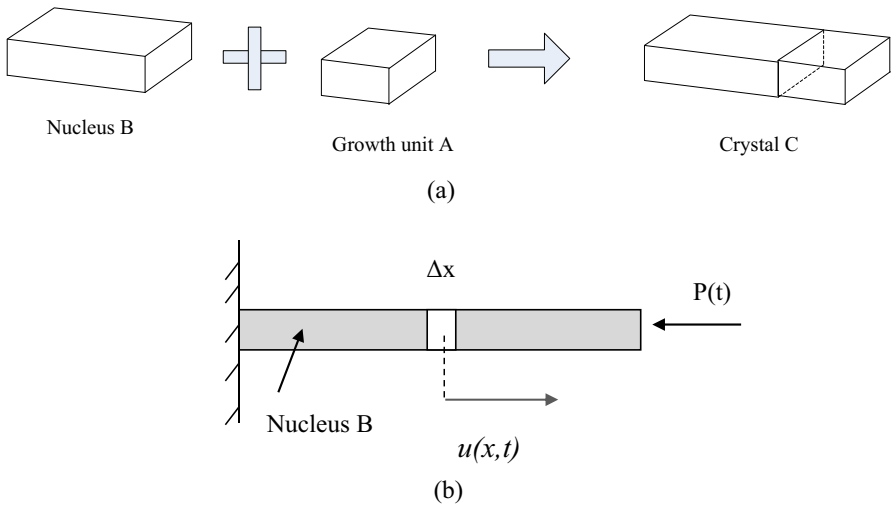

Figure 4: (a) Three-dimensional schematic diagram of crystal C is obtained by combining growth unit A and nucleus B; (b) schematic view of elastic nucleus B undergoing axial motions.

1,000 s, the AE become less, because of collision and friction between the crystals.

As shown in Figure 3, from about 150 s, several frequency signals are observed. This observation means that there is crystal nucleation. From about 200 to 400 s, huge amounts of emission acoustic signals are observed. There are lots of crystals nucleation and growth. After 600 s, the emission acoustic signal tends to several frequencies. Crystal growth is indeed the basic permanent crystal phenomenon in the process from about 150 s to the end.

In the following sections, a mechanics model is used to calculate the frequency of the AE signal released during the crystal growth stage of salicylic acid. According to the diffusion theory of Noyes, Whitney, and Nernst [53,54], the matter is deposited on the crystal surface continuously at a rate proportional to the concentration difference between the surface and the bulk solution.

Thanks to Landau Lifchitz, *Theory of Elasticity: Volume 7* (*Theoretical Physics*), Chapter: 25, this section sets up the relation between emission acoustic frequency and crystallization. The vibration of crystals leads to the emission of acoustic signals. As shown in Figure 4, a particle is fixed on the left end side, and the right end is free. A force is applied to the right side. It is assumed that the elastic displacement of $u(x,t)$ is produced by the force $P(t)$ acting on the free end of particle a. Considering the basic strength of particles, we assume that the cross-section of particles is perpendicular to the x-axis of the spindle and the cross-sectional area is A. The particle is linear elastic and its properties (ρ, E) are homogeneous at any given cross-section. When a force is applied to the right side of the particle, the particle will begin vibrating. This vibration leads to the AE signal. During crystallization (nucleation, growth), when the growth unit A joins the nucleus B, as shown in Figure 4a, the two particles grow to crystal C. This phenomenon is similar to that in Figure 4b, growth unit A gives a force to the nucleus B. Nucleus B begins to vibrate. The three-dimensional structure diagram of the process of growth unit A combining with nucleus B is approximately represented in Figure 4a, and a schematic view of elastic nucleus B undergoing axial motions is represented in Figure 4b. Vibration frequencies of crystal growth will be calculated in the following section.

Consider the free body diagram of an infinitesimally small piece of a particle with length Δx, $P(x,t)$ is the axial force at a cross-section of the particle.

Applying Newton's second law of motion on the growth unit differential element gives

$$\sum_x F_x = \Delta m a_x = (\rho A \Delta x) \frac{\partial^2 u}{\partial t^2}, \tag{1}$$

where the left side of the equation is the sum of all forces acting on the infinitesimally small piece of a particle along the x-direction, Δm is the mass of the infinitesimally small piece of a particle along the x-direction, a_x is the acceleration along the x-direction, ρ is the density of the particle, A is the cross-sectional area of the particle, Δx is the length of the infinitesimally small piece of particle, and $u(x,t)$ is the elastic displacements of the particle caused by the force $P(t)$ at time t.

In the present case, the unique force acting at the free end of the particle is P. Therefore, equation (1) can be written as follows:

$$(\rho A\Delta x)\frac{\partial^2 u}{\partial t^2} = P_{(x+\Delta x,t)} - P_{(x,t)}. \tag{2}$$

By the definition of limit, as $\Delta x \to 0 \Rightarrow P_{(x+\Delta x,t)} \approx P_{(x,t)} + \frac{\partial P}{\partial x}\Delta x$, and replacing $P_{(x,t)} = AE\frac{\partial u}{\partial x}$, the following equation can be obtained:

$$\rho A\frac{\partial^2 u}{\partial t^2} = \frac{\partial}{\partial x}\left(AE \cdot \frac{\partial u}{\partial x}\right). \tag{3}$$

The solution of partial differential equation (PED) (3) is of the form:

$$u_{(x,\,t)} = \varnothing_{(x)} v_{(t)}. \tag{4}$$

Substitution of the product solution equation (4) into PDE (3) gives

$$\frac{\rho}{E}\frac{\partial^2 u}{\partial t^2} = \frac{\partial^2 u}{\partial x^2} \;\rightarrow\; \frac{\rho}{E}\varnothing_{(x)}\ddot{v}_{(t)} = \varnothing''_{(x)}\, v_{(t)}. \tag{5}$$

The above formula is based on the assumption that all points on the particle move synchronously. By using the method of separating variables, $u(x,t)$ is decomposed into the product of two functions $\varnothing_{(x)}$ and $v_{(t)}$. The function $\varnothing_{(x)}$ describes the longitudinal vibration amplitude of the cross-section on the particle at the distance from the origin x. The function $v_{(t)}$ describes the variation of the vibration of each section with time.

With the definitions $\dot{(\cdot)} = \frac{\mathrm{d}}{\mathrm{d}t}$ and $(') = \frac{\mathrm{d}}{\mathrm{d}x}$. For a particle with uniform material properties (ρ, E) and cross-section A, the substitution of the product solution equation (4) into PDE (3) gives

$$\frac{\ddot{v}_{(t)}}{v_{(t)}} = \frac{E}{\rho}\frac{\varnothing''_{(x)}}{\varnothing_{(x)}}. \tag{6}$$

Above, the left-hand side is only a function of time, while the right-hand side is only a function of spatial coordinate x. This is possible only if both sides equal to a constant. It can be written as follows:

$$\frac{\ddot{v}_{(t)}}{v_{(t)}} = \frac{E}{\rho}\frac{\varnothing''_{(x)}}{\varnothing_{(x)}} = -\omega^2. \tag{7}$$

Hence, the PDE is converted into two ordinary differential equations (ODEs):

$$\ddot{v}_{(t)} + \omega^2 v = 0, \tag{8}$$

$$\varnothing''_{(x)} + \lambda^2\varnothing_{(x)} = 0, \tag{9}$$

where

$$\lambda = \omega\sqrt{\rho/E}\,.$$

The solution of the ODEs (8) and (9) is

$$v_{(t)} = C_t\,\cos(\omega t) + S_t\,\sin(\omega t), \tag{10}$$

$$\varnothing_{(x)} = C_x\,\cos(\lambda x) + S_x\,\sin(\lambda x), \tag{11}$$

where C_t , C_x, S_t, and S_x are determined by boundary conditions. In this case, the boundary conditions are as follows:

$$\text{At } x = 0, \quad u_{(0,\,t)} = 0 = \varnothing_{(0)} v_{(t)} \rightarrow \varnothing_{(0)} = 0\ \forall t.$$

$$\text{At } x = L, \quad \left.\frac{\partial u}{\partial x}\right|_{x=L} = 0 = \varnothing'_{(L)}\, v_{(t)} \;\rightarrow\; \varnothing'_{(L)} = 0\ \forall t,$$

where L is the length of the particle.

Hence, from the characteristic equation $\varnothing_{(0)} = 0 \;\rightarrow\; C_x = 0$.

Note that $S_x \neq 0$ for a nontrivial solution. Hence, the characteristic equation for axial motions of a fixed end–free end elastic growth unit is

$$\cos(\lambda L) = 0. \tag{12}$$

Hence, the roots of equation (12) are

$$\lambda_n = \frac{(2n-1)}{2}\frac{\pi}{L}, \quad n = 1, 2\ \ldots. \tag{13}$$

And since $\lambda = \omega\sqrt{\frac{\rho}{E}}$, the natural frequencies of the fixed end–free-end growth unit are

$$\omega_k = \frac{(2k-1)}{2}\frac{\pi}{L}\left(\frac{E}{\rho}\right)^{1/2}. \tag{14}$$

Hence, we obtained the formula for calculating the vibration frequencies generated by the combination of particles and crystallization nucleation [55].

$$f_k = \frac{(2k-1)}{4L}\left(\frac{E}{\rho}\right)^{1/2}, \quad k = 1, 2,\ldots. \tag{15}$$

The particle size with the injection rate of 20.8 mL/min is about 600 to 1,100 μm [24]. The density and Young's modulus of salicylic acid are $\rho = 1.376 \times 10^3$ kg/m^3 and $E = 1$ GPa, respectively [56]. The Young's modulus at zero porosity of the various drugs ranges from 0.71 to 8.73 GPa. By introducing the above-known conditions into formula (15), the range of vibration frequencies can be calculated to be 355–200 kHz. The smaller the grain size is, the greater the vibration frequency is, which is beyond the maximum range of 350 kHz set by our experiment. It cannot be collected, so here the particle sizes between 600 and 1,100 μm are used to calculate the particle sizes distribution as shown in previous research [24]. The corresponding vibration frequencies are 200–355 kHz, which are consistent with the experimental results as shown in Figure 5.

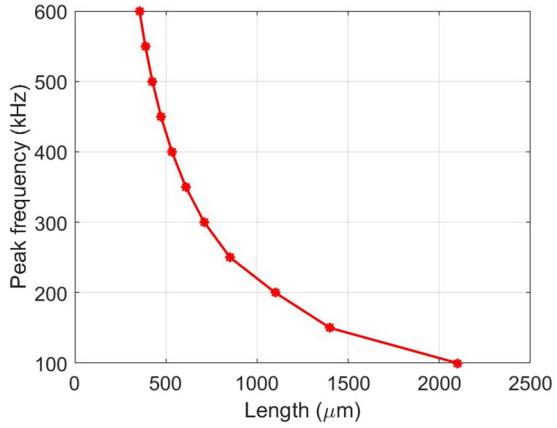

Figure 5: The particle length corresponding to vibration frequencies.

5 Further discussion

A time and frequency domain analysis was performed to get an additional point of view on the crystallization process. As shown in Figure 6, the frequency range was divided into samples of width 10 kHz, (0–10 kHz, 10–20 kHz, 390–400 kHz). In order to reduce the amount of acoustic data and to compute a smooth $(t, \overline{f},\ a\bar{E}_{i,j})$ surface plot, every time domain was divided into 10 s sample. Therefore, the size of the time–frequency grid was [100 × 40], frequency and time domains were divided into 40 intervals (0–400 kHz) and 70 intervals (0–1,000 s), respectively. Thus, the time–frequency domain was cut into 4,000 cells. Every time–frequency cell was filled by the corresponding absolute energy value $a\bar{E}_{i,j}$ computed as

$$a\bar{E}_{i,j} = \frac{\sum_{k=1}^{N_{i,j}} E_k}{\Delta f \cdot \Delta t}, \tag{16}$$

where E_k is the value of the absolute energy of hit n^0k located inside the cell $[i, j]$, $N_{i,j}$ is the total number of hits inside the same cell, and Δf and Δt are the frequency and time intervals defining the size of the $[i, j]$ grid, respectively.

Figure 6 shows the 3D plot of the average absolute acoustic energy recorded in the frequency domain (0–400 kHz). A significant level of energy can be observed at 150 to 180 s and the corresponding peak frequency related to the maximum AE energy is located around 260 kHz. Figure 6 also shows that the energy becomes negligible after 400 s. As shown in Figure 6, the AE

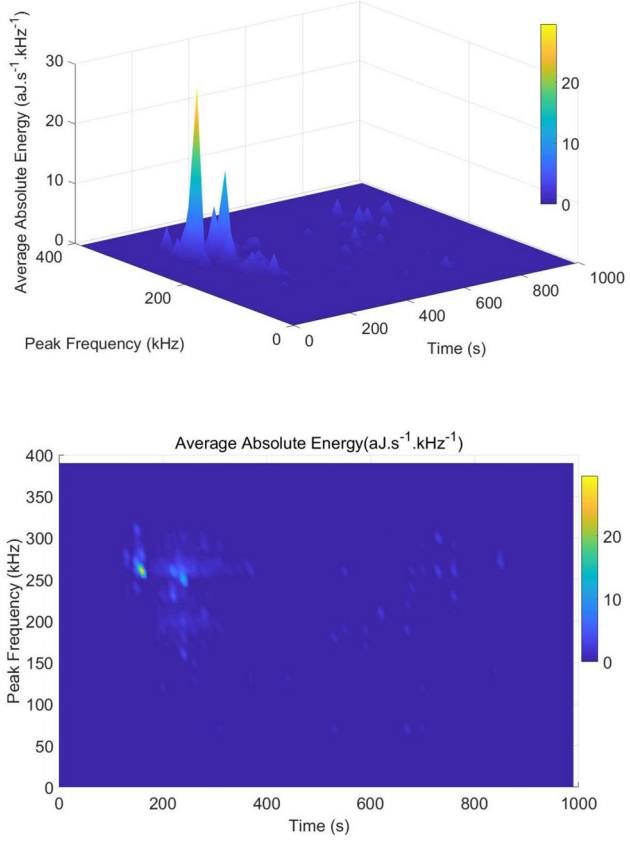

Figure 6: Average absolute energy E_{abs}, as a function of the peak frequency and time.

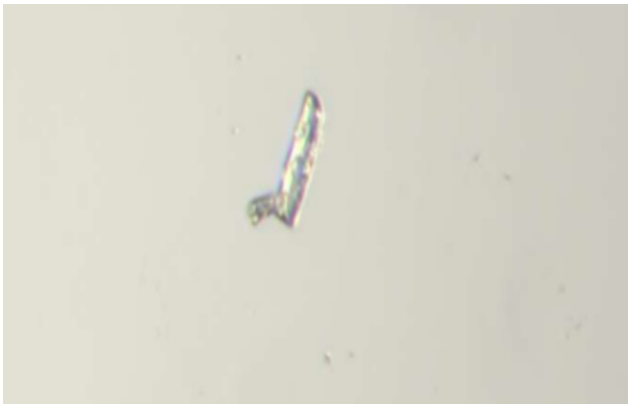

Figure 7: Grain size of salicylic acid.

signals vary from 250 to 300 kHz and the crystal size corresponds to 852–710 μm.

The beginning of the AE activity in the frequency domain 260 kHz could be expected to correspond to the beginning of nucleation and crystal growth. The outbreak of AE activity at time 200 s precedes the two-dimensional nucleus and three-dimensional nucleation [57]. It seems again reasonable to conclude that AE allows detecting the onset of nucleation much before the solids generation process becomes significant. One can therefore assume that the absolute energy recorded in the frequency domain investigation is related to the rate of crystal nucleation and growth. The end of the AE activity under investigation could be expected to be the end of the chemical reaction. More details of physical explanation could be found in previous research [24].

The final grain of salicylic acid is shown in Figure 7. The shape of the salicylic acid could be considered as a cylinder. Although there are several components of the wave traveling in a solid, this article uses a simple 1D analysis to set up the relationship between AE frequency and particle size. Future work is focused on different waves corresponding to the AE frequency.

6 Conclusion

In this article, the corresponding relationship between AE frequency and particle size has been set up by analyzing the collected AE signals.

1. The vibration frequencies of particles (600–1,100 μm) calculated by the proposed formula are in good agreement with the experimental results (200–355 KHz).
2. Once the relationship between AE frequency and crystal particle size is established, the formula can be used to predict the particle size.

This method can be used to monitor the crystallization process to obtain the required crystal size and particle distribution, to achieve the desired final product quality. AE signal during the process of crystal nucleation and its vibration model are further studied in future work.

Funding information: The presented work was supported by the National Natural Science Foundation of China (grant nos. 51808554).

Author contributions: All authors have accepted responsibility for the entire content of this manuscript and approved its submission.

Conflict of interest: The authors state no conflict of interest.

References

[1] Zhang S, Liang Y, Qian X, Hui D, Sheng K. Pyrolysis kinetics and mechanical properties of poly(lactic acid)/bamboo particle biocomposites: effect of particle size distribution. Nanotechnol Rev. 2020;9:524–33.
[2] Variankaval N, Cote AS, Doherty MF. From form to function: crystallization of active pharmaceutical ingredients. AIChE J. 2008;54:1682–8.
[3] Cheng C, Song W, Zhao Q, Zhang H. Halloysite nanotubes in polymer science:purification, characterization, modification and applications. Nanotechnol Rev. 2020;9:323–44.
[4] Takiyama, H. Supersaturation operation for quality control of crystalline particles in solution crystallization. Adv Powder Technol. 2012;23:273–8.
[5] Przybyłek M, Cysewski P, Pawelec M, Ziółkowska D, Kobierski M. On the origin of surface imposed anisotropic growth of salicylic and acetylsalicylic acids crystals during droplet evaporation. J Mol Modeling. 2015;(21):49–61.
[6] Oku T. Crystal structures of perovskite halide compounds used for solar cells. Rev Adv Mater Sci. 2020;59:264–305.
[7] Révész D, Horváth A, Ribárik G, Schafler E, Kovács Z. Crystallization of $Cu_{60}Zr_{20}Ti_{20}$ bulk metallic glass by high pressure torsion. Rev Adv Mater Sci. 2019;58:304–12.
[8] Jahangir A, Malik F, Muhammad N, Fayyaz R, Abbasi JN, Nazir A. Reflection phenomena of waves through rotating elastic medium with micro-temperature effect. Rev Adv Mater Sci. 2020;59:455–63.
[9] Ment T, Ying K, Hong Y, Xu Q. Effect of different particle sizes on nano-SiO_2 on the properties and microstructure of cement paste. Nanotechnol Rev. 2020;9:833–42.
[10] Greaves D, Boxall J, Mulligan J, Montesi A, Creek J, Sloan ED, et al. Measuring the particle size of a known distribution using the focused beam reflectance measurement technique. Chem Eng Sci. 2008;63:5410–9.
[11] Yu W, Erickson K. Chord length characterization using focused beam reflectance measurement probe – methodologies and pitfalls. Powder Technol. 2008;185:24–30.

[12] Wynn EJW. Relationship between particle-size and chord-length distributions in focused beam reflectance measurement: stability of direct inversion and weighting. Powder Technol. 2003;133:125–33.
[13] Nishioka Y, Ohsawa T, Kobayashi M, Noda K. Laser diffraction estimation of particle size distribution of slightly water-soluble drugs coexisting with additives: application to solid dosage forms. Chem Pharm Bull. 1992;40:1563–8.
[14] Ma Z, Merkus HG, Smet J, Heffels C, Scarlett B. New developments in particle characterization by laser diffraction: size and shape. Powder Technol. 2000;111:66–78.
[15] Linton RW, Williams P, Evans CA. Determination of the surface predominance of toxic elements in airborne particles by ion microprobe mass spectrometry and Auger electron spectrometry. Anal Chem. 1997;49:1514–21.
[16] Dhodapkar SV, Klinzing GE. Pressure fluctuations in pneumatic conveying systems. Powder Technol. 1993;74:179–95.
[17] Subero-Couroyer C, Mangin D, Rivoire A, Blandin AF, Klein JP. Agglomeration in suspension of salicylic acid fine particles: analysis of the wetting period and effect of the binder injection mode on the final agglomerate size. Powder Technol. 2006;161:98–109.
[18] Hatkar UN, Gogate PR. Process intensification of anti-solvent crystallization of salicylic acid using ultrasonic irradiations. Chem Eng Process Process Intensif. 2012;57–58:16–24.
[19] Seidel J, Ulrich J. Generation of crystalline microcontainers of salicylic acid. Chem Eng & Technol. 2015;38:984–90.
[20] Martins D, Stelzer T, Ulrich J, Coquerel, G. Formation of crystalline hollow whiskers as relics of organic dissipative structures. Cryst Growth Des. 2011;11:3020–6.
[21] Caro JA, Woldehaimanot M, Rasmuson ÅC. Semibatch reaction crystallization of salicylic acid. Chem Eng Res Des. 2014;92:522–33.
[22] Wang XJ, Févotte G, Huang Y, Michelitsch TM. Acoustic emission during the solvent mediated cooling crystallization of citric acid. Powder Technol. 2016;301:70–7.
[23] Wang XJ, Huang Y, Michelitsch TM. Acoustic emission detection of crystallization in two forms: monohydrate and anhydrous citric acid. Pharm Dev Technol. 2019;24:419–26.
[24] Wang XJ, Huang Y. An investigation of the acoustic emission generated during crystallization process of salicylic acid. Powder Technol. 2017;311:350–5.
[25] Kusnierz J, Pawelek A, Ranachowski Z, Piatkowski A, Jasienski Z, Kudela S. Mechanical and acoustic emission behaviour induced by channel-die compression of Mg-Li nanocrystalline alloys obtained by ecap technique. Rev Adv Mater Sci. 2008;12:583–9.
[26] Albion K, Briens L, Briens C, Berruti F. Detection of the breakage of pharmaceutical tablets in pneumatic transport. Int J Pharma. 2006;322:119–29.
[27] Albion K, Briens L, Briens C, Berruti F, McDougall S. Detection of oversized material in a hydrotransport slurry pipe using a non-invasive acoustic method. Powder Technol. 2009;190:361–71.
[28] Allan P, Bellamy LJ, Nordon A, Littlejohn D. Non-invasive monitoring of the mixing of pharmaceutical powders by broadband acoustic emission. Analyst. 2010;135:518–24.
[29] Nordon A, Waddell RJH, Bellamy LJ, Gachagan A, McNab D, Littlejohn D, et al. Monitoring of a heterogeneous reaction by acoustic emission. Analyst. 2004;129:463–7.
[30] Nordon A, Carella Y, Gachagan A, Littlejohn D, Hayward G. Factors affecting broadband acoustic emission measurements of a heterogeneous reaction. Analyst. 2006;131:323–30.
[31] Vervloet D, Nijenhuis J, van Ommen JR. Monitoring a lab-scale fluidized bed dryer: a comparison between pressure transducers, passive acoustic emissions and vibration measurements. Powder Technol. 2010;197:36–48.
[32] Wang JD, Ren CJ, Yang YR. Characterization of flow regime transition and particle motion using acoustic emission measurement in a gas–solid fluidized bed. AIChE. 2010;56:1173–83.
[33] Zhou YF, Dong KZ, Zhengliang H, Wang JD, Yang YR. Fault detection based on acoustic emission-early agglomeration recognition system in fluidized bed reactor. Ind Eng Chem Res. 2011;50:8476–84.
[34] Matero S, Poutiainen S, Leskinen J, Järvinen K, Ketolainen J, Reinikainen SP, et al. The feasibility of using acoustic emissions for monitoring of fluidized bed granulation. Chemom Intell Lab Syst. 2009;97:75–81.
[35] Stamm M, Pfeiffer H, Reynaert J, Wevers M. Using acoustic emission measurements for Ice-melting detection. Appl Sci. 2019;9:5387.
[36] Zhang X, Xin BJ, Zheng YS, Shi MW, Lin LT, Gao C, et al. Study on fiber fracture sequence during yarn tensile fracture via acoustic emission method. J Text Inst. 2021;112:417–28.
[37] Daniher D, Briens L, Tallevi A. End-point detection in high-shear granulation using sound and vibration signal analysis. Powder Technol. 2008;181:130–6.
[38] Gamble JF, Dennis AB, Tobyn M. Monitoring and end-point prediction of a small scale wet granulation process using acoustic emission. Pharm Dev Technol. 2009;14:299–304.
[39] Briens L, Daniher D, Tallevi A. Monitoring high-shear granulations using sound and vibration measurements. Int J Pharma. 2007;331:54–60.
[40] Hansuld EM, Briens L, McCann JAB, Sayani A. Audible acoustics in high-shear wet granulation: application of frequency filtering. Int J Pharma. 2009;378:37–44.
[41] Sawada T, Gohsi Y, Abe C, Furuya K. Acoustic emission from phase transition of some chemicals. Anal Chem. 1985;57:1743–5.
[42] Ersen A, Smith A, Chotard T. Effect of malic and citric acid on the crystallization of gypsum investigated by coupled acoustic emission and electrical conductivity techniques. J Mater Sci. 2006;41:7210–7.
[43] Lube EL, Zlatkin AT. In-process monitoring of crystal perfection during melt growth. J Cryst Growth. 1989;98:817–26.
[44] Yaroslavkina E, Tyurin E, Zobnin P, Melnikov E. Acoustic emission system for studing the effect of AlTi5Bi modifier on the crystallization of aluminum. International Conference Complex Systems: Control and Modeling Problems (CSCMP). Samara, Russia: IEEE; 2019.
[45] Safaei B. The effect of embedding a porous core on the free vibration behavior of laminated composite plates. Steel Comp Struct. 2020;35:659–70.
[46] Li H, Lv H, Sun H, Qin Z, Xiong J, Han Q, et al. Nonlinear vibrations of fiber-reinforced composite cylindrical shells with bolt loosening boundary conditions. J Sound Vib. 2021;496:115935.
[47] Moradi-Dastjerdi R, Behdinan K, Safaei B, Qin Z. Static performance of agglomerated CNT-reinforced porous plates bonded with piezoceramic faces. Int J Mech Sci. 2020;188:105966.

[48] Moradi-Dastjerdi R, Behdinan K, Safaei B, Qin Z. Buckling behavior of porous CNT-reinforced plates integrated between active piezoelectric layers. Eng Struct. 2020;222:111141.
[49] Sahmani S, Safaei B. Large-amplitude oscillations of composite conical nanoshells with in-plane heterogeneity including surface stress effect. Appl Math Model. 2021;89:1792–1813.
[50] Ying L, Li L. Understanding the corrosion resistance of nanocrystalline materials: electrochemical influences. Corrosion protection and control using nanomaterials. Woodhead Publishing; 2012. p. 59–85.
[51] Bloch L, Kauffmann Y, Pokroy B. Size effect on the short range order and the crystallization of nanosized amorphous alumina. Cryst Growth Des. 2014;14:3983–9.
[52] Mosivan S, Kazeminezhad I. Magnetite nanoparticles functionalized with polypyrrole by pulsed sono-electrocrystallization and their applications for water treatment. J Mater Sci Mater Electron. 2018;29:12466–76.
[53] Jiang Q, Tallury S, Qiu Y. Interfacial characteristics of a carbon nanotube-polyimide nanocomposite by molecular dynamics simulation. Nanotechnol Rev. 2020;9:136–45.
[54] Thompson L, Azadmanjiri J, Nikzad M, Sbarski I, Wang J, Yu A. Cellulose nanocrystals: production, functionalization and advanced applications. Rev Adv Mater Sci. 2019;58:1–16.
[55] Lifchitz EM, Kossevitch A, Pitayevski LP. Transl, theoretical physics. Vol. 7. Theory of elasticity. From the Russian by V. kolimeev. 2nd ed. Moscow: Editions Mir. 264 P; 1990.
[56] Roberts RJ, Rowe RC, York P. The relationship between young modulus of elasticity of organic-solids and their molecular-structure. Powder Technol. 1991;65:139–46.
[57] Mullin JW. Crystallization. 3rd ed. Oxford: Butterworth-Heinemann; 1993. p. 205